Water Does Not Dance as Ions Sing: a New Approach in Elucidation of Ion-Invariant Water Fluctuations

Zlatko Brkljača[a, *], Marija Butumović[b], Danijela Bakarić[a, *]

[a] Division for Organic Chemistry and Biochemistry, Ruđer Bošković Institute, Bijenička 54, 10000 Zagreb, Croatia

[b] Division of Analytical Chemistry, Department of Chemistry, Faculty of Science, University of Zagreb, Horvatovac 102a, 10000 Zagreb, Croatia

Abstract

Aqueous solutions of salts composed from monovalent ions are explored using temperature-dependent FT-IR spectroscopy in transmission. Water combination band, being extremely sensitive to the network of hydrogen bonds due to the contribution of water librations ($\rho_L H_2O$), is analyzed in uni- and multivariate fashion. Univariate analysis of the combination band maximum (ν_{max}) reveals that perturbation of water hydrogen bond network by ions is primary driven by electrostatic interactions between water and ions. Using multivariate curve resolution with alternating least squares and evolving factor analysis this band is separated into two components that represent low- and high-density water. The observed asymmetry in their behavior is interpreted in terms of fluctuations of a hydrogen bond network of two water components. The significance of the found phenomenon is unambiguously confirmed by performing analogous analysis in the spectral range that contains partial signature of water linear bending (δHOH) and is free from $\rho_L H_2O$, in which the asymmetry is absent. Additionally, we show that this phenomenon, namely ion-invariant behavior of water fluctuations, persists even in the regime of high ionic strengths. Although ions indeed participate in shaping of water hydrogen bond network, this straightforward approach shows that its temperature-dependent fluctuations are ion-independent.

Keywords: Water; Salts; Temperature-dependent transmission FT-IR spectra, Combination band; Multivariate curve resolution method; Fluctuations

1. Introduction

Permeating all segments of the biosphere, water (H_2O) is considered to be the most important liquid substance on Earth [1–5]. Among the physicochemical properties of water that reflect its anomalous behavior, its maximum density (ρ) at 4 °C, isothermal compressibility (κ_T) that decreases upon heating up to 46 °C, above which it starts to rise, and its heat capacity at constant pressure (C_p) displaying an increase below 35 °C stand out [6]. These anomalous macroscopic properties presumably originate from the coexistence of discrete water microstructures, commonly defined via the geometry of hydrogen bond network [7,8], whose distribution largely depends on the environmental conditions [7–10]. As demonstrated by FT-IR spectroscopy, in its condensed phase, both hydrogen bond donors (H-atoms) and both hydrogen bond acceptor (lone-electron pairs on O-atom) sites almost fully participate in creating water hydrogen bond network [5,11] making non-hydrogen-bonded OH groups virtually insignificant species (< 5 %) [5,12,13].

Due to the exceptional ability of water OH moieties in forming hydrogen bonds, linear FT-IR spectroscopy has deservedly been placed in the focus of investigating the temperature dependence of water microstructures [5]. Applying principal component analysis (PCA) and partial least squares (PLS) regression on $\nu_{(anti)sym}$OH bands of liquid water, Libnau et al. deduced that in temperature range 2 – 96 °C two water microstructures exist, differing by ~ 0.5 hydrogen bonds [14,15]. Thermal evolution of the water signatures in medium- and near-IR range (MIR and NIR, respectively) was additionally analyzed by the combination of multivariate curve resolution with alternating least squares and evolving factor analysis (MCR-ALS with EFA) and two-dimensional correlation spectroscopy (2DCOS) [16]. In the two aforementioned water microstructures, discriminated dominantly by the number of hydrogen bonds, the authors managed to identify even non-hydrogen-bonded water molecules. Despite the intrinsic limitations of various experimental and computational techniques, along with ambiguities arising from the interpretation of obtained data related with hydrogen bond stoichiometry [17–19], there is a universal consensus that microscopic structure of water at ambient conditions is based on tetrahedral arrangement of water molecules that decreases with increasing temperature [20]. Furthermore, all studies have shown that the change of temperature inevitably disorders hydrogen bond network and induces microstructure fluctuations.

Besides the temperature, hydrogen bond network structure [21,22] and dynamics [21,23–25] can be disturbed to the certain extent by the presence of solutes as simple as ions [26–29]. For instance, Na^+ and K^+ ions, which are similar in size to water molecules, only slightly disturb hydrogen bond network in structural terms, however, their presence is found to change the flexibility of a hydrogen bond network [5]. Ion contribution to the strengthening or weakening of the hydrogen bond network (kosmotropes and chaotropes, respectively) [30–34] has been intensively explored by computational and spectroscopic techniques [26,35–38]. Although the envelope generated by $\nu_{(anti)sym}OH$ is universally considered as the signature with the richest response of water hydrogen bond network [26,29,37,39,40], band arising from the linear bending of water (δHOH) [41] and especially combination band, [42] originating from a fundamental transition of δHOH and water librations ($\rho_L H_2O$), [43] gained considerable attention over the last years in this respect. Unlike $\nu_{(anti)sym}OH$ (~ 3300 cm^{-1}) and δHOH (~ 1650 cm^{-1}), representing intramolecular normal modes, $\rho_L H_2O$ are intermolecular normal modes which in liquid water appear at about 700 cm^{-1} due to the strong hydrogen bonds between water molecules [5]. As this frequency coincides with the bending of hydrogen bonds, they are also described as hindered rotations of water molecules, thus being extremely sensitive to changes in temperature [5] and molecular surroundings [44,45]. Recently Verma et al. analyzed the changes in the combination band position maximum (ν_{max}; ~ 2130 cm^{-1}) as a function of various salts and their concentration [46]. As concentration-dependent band maximum displays low- and high-frequency shift for chaotropes and kosmotropes, respectively, their general conclusion was that combination band can be used as a probe for monitoring both local and collective dynamics of water. Consequently, it is reasonable to assume that the band containing the signature of water librations, when examined in temperature-dependent manner, can be used as a probe for deciphering ion-induced fluctuations of water hydrogen bond network.

This study presents a new approach in identifying the impact of ions on water microstructure and on fluctuations of the associated hydrogen bond network, regardless of the arrangement of water molecules. Starting from the assumption that in certain temperature range there are two types of water, high- and low-density water, we show that the analysis of the components concentration profiles, obtained using MCR-ALS coupled with EFA, provides deeper insight compared to just the usual application which determines the presence or absence of a particular component. More specifically, by regression of concentration profiles on a polynomial of a certain degree,

asymmetry between high- and low-density water is observed depending on whether the spectral region under investigation contains the signature of water librations. Since librations are intimately related with the hydrogen bond network, the noticed asymmetry is found to be caused by the fluctuations in water microstructures in high- and low-density water. We thus found that, although ions participate in the formation of a hydrogen bond network in terms of multipole interactions [47,48], instead in terms of their kosmotropic/chaotropic classification as previously stated [46], the hydrogen bond network perturbations are effectively unchanged with the addition of ionic species. The validity of our findings, which are based on defining the completely new terms of temperature-dependent water hydrogen bond network fluctuations, is supported by the results obtained from femtosecond elastic second harmonic scattering (fs-ESHS) experiments conducted on aqueous salt solutions [49].

2. Experimental

2.1 Chemicals and solutions preparations

Sodium chloride (NaCl; white powder, Gram mol, p. a.), sodium bromide (NaBr; white powder, Kemika, p. a.), sodium iodide (NaI, white powder, Kemika, 99 %), sodium nitrate ($NaNO_3$; white crystals, AnalaR, 99 %), sodium nitrite ($NaNO_2$; white crystals, Kemika, p. a.), sodium acetate (CH_3COONa; white powder, Kemika, p. a.), sodium hydroxide (NaOH; white pearls, Kemika, p. a.), potassium chloride (KCl; white powder, Kemika, p. a), potassium bromide (KBr; white powder, Acros Organics, 99+ %), potassium iodide (KI, white powder, Kemika, p. a.), potassium nitrate (KNO_3; white powder, Merck, p. a.), potassium nitrite (KNO_2; transparent crystals, Merck, p. a.), potassium acetate (CH_3COOK; white powder, Kemika, p. a.) and potassium hydroxide (KOH; white pellets, Kemika, p. a.), were used as received (their purities were checked by recording the spectra of powders and comparing with the reference data, see Supporting Information, Fig. S1). Aqueous solutions of these salts in milli-Q water of ionic strength I = 1 M were prepared. pH values of milli-Q water and prepared aqueous solution of chlorides (Na^+ / K^+), bromides (Na^+ / K^+), iodides (Na^+ / K^+) and nitrates (Na^+ / K^+) (measured by pH tester, Hanna Instruments) were ≈ 6.5; for salts of nitrites ≈ 6.9 (Na^+) and ≈ 7.8 (K^+); for acetates ≈ 8.4 (Na^+ / K^+); for hydroxides ≈13 (Na^+) and ≈ 14 (K^+). In order to estimate the impact of solution pH value on the combination band and general spectral features, solutions of hydroxides (Na^+ and K^+) were measured in concentration range 0.001 M ≤ c (NaOH / KOH) ≤ 1 M (the spectra are presented in

Supporting Information, Fig. S2). Overall, pH values of dilute solutions of NaOH and KOH (0.001 M ≤ *c* (NaOH / KOH ≤ 0.01 M) are very close to the pH value of pure water (pH values are provided in Table S1, section S2 in Supporting Information) and the FT-IR spectra of solutions of hydroxides appears to be virtually identical to the spectrum belonging to pure water. For *c* (NaOH / KOH) ≥ 0.1 M pH is significantly larger and for *c* (NaOH / KOH) = 1 M pH is ~13 / ~ 14, respectively, thus significant differences in their FT-IR spectra compared to pure water FT-IR spectrum appear (see discussion in section S2, Supporting Information).

2.2 FT-IR spectroscopy

2.2.1 FT-IR spectra acquisition of aqueous solutions of salts

FT-IR spectra of aqueous solutions were measured on an ABB Bomem MB102 spectrometer equipped with CsI optics and a DTGS detector in a transmission in a sealed cell equipped with CaF_2 windows with the path length of the cell d = 48.48 μm, which was determined interferometrically. Temperature was regulated by Specac 3000 Series high stability temperature controller with heating jacket. Solutions were recorded in the temperature range 25 – 70 °C every 5 °C with the heating rate of 5 °C min^{-1}. All spectra were collected with nominal resolution of 2 cm^{-1} and 10 scans. These conditions are considered optimal for collecting spectra of aqueous solutions that are minimally compromised by the change in atmosphere (CO_2 and H_2O vapor) during the measurement (more details are presented in Supporting Information, section S3). Every solution was recorded three times.

2.2.2 FT-IR spectra analysis

FT-IR spectra were divided and examined in two spectral ranges: i) 2650–1800 cm^{-1} (D_1) containing water combination band and ii) 1560–1260 cm^{-1} (D_2) that, besides containing partial signature of δHOH band, is free from absorption and, more importantly, free from water librations. In D_1 spectral region the baseline correction is drawn through the signal minima (at 2600 cm^{-1} and 1850 cm^{-1}, see raw FT-IR spectra in Fig. S3 in Supporting Information), whereas a vertical setoff with minimum at 1380 cm^{-1} is made as a baseline correction in D_2 spectral range. Following the baseline correction the spectral response was smoothed using Savitzky-Golay filter [50]. Due to the contamination of combination band with uncontrollable atmospheric CO_2 signature ($\nu_{as}CO_2$

with maximum at about 2350 cm^{-1}, see Fig. S3 in Supporting Information), multivariate analysis was conducted on spectral range 2300–1800 cm^{-1}.

Univariate analysis was conducted on D_1 spectral range with the aim of determining the position of the band maximum (ν_{max}) as a function of temperature. As ν_{max} displays linear decrease with temperature, linear regression of this data set $y = B_0 + B_1 \cdot x$ provides ν_{max} at 0 °C (B_0) and the rate of wavenumber decrease (B_1). When placed in physicochemical context, B_0 (ν_{max} at 0 °C or $\nu_{max,\,0}$) gives the average position of combination band of water molecules in which hindered rotations are significantly reduced. Furthermore, B_0 reflects the strength of the hydrogen bond network in the presence of particular ions and enables the comparison with the analogous quantity obtained from FT-IR spectra of pure water.

Multivariate analysis. MCR-ALS with EFA is a statistical tool that enables determination of the spectral and concentration profiles of the components in the system without a prior knowledge of their signal shape, position or identity [51]. In mathematical terms, it decomposes data matrix (**D**) into the matrices of spectral (**S**) and concentration (**C**) profiles of particular component by solving following system of equations:

$$\mathbf{D}=\mathbf{C}\mathbf{S}^{\mathbf{T}}+\mathbf{E} \qquad (1)$$

with **E** being the matrix of residuals unexplained by the species found in **S** and **C**.

In aqueous systems prepared here we were focused on multivariate analysis of two spectral regions (D_1 and D_2). Their constitutive data matrices ($\mathbf{D_1}$ and $\mathbf{D_2}$) contain spectral responses at different temperatures (rows) and different wavenumber (wavenumbers). Since the FT-IR spectra are acquired at ten different temperatures, the number of rows (N_r) in both $\mathbf{D_1}$ and $\mathbf{D_2}$ is, accordingly, ten, whereas the number of columns (N_c) varies with the number of wavenumbers in particular spectral region ($\mathbf{D_1}$ contain 519 points and $\mathbf{D_2}$ 312 points). Thus, dimensions of the prepared matrices ($N_r \times N_c$) are 10 × 519 and 10 × 312, respectively.

The first step in obtaining the spectral and concentration profiles of particular component is to make an initial estimate of their number in order to determine the system rank. This is usually performed using mathematical procedures/algorithms such as singular value decomposition (SVD). Once the initial number of components is found, EFA is applied on the constructed data

matrix ($\mathbf{D_i}$; i = 1, 2) in order to follow the change of data matrix rank as a function of an ordered variable. This is carried out by making singular value decomposition of $\mathbf{D_i}$ submatrices that are obtained by adding the rows of $\mathbf{D_i}$ successively, starting either from the first (forward; 1, 2, 3, ..., N_r rows) or from the last (backward; N_r, N_{r-1}, N_{r-2}, ..., 1 row) row of the original data matrix $\mathbf{D_i}$. By performing EFA in both directions the information of the appearance and disappearance of the individual components is complete and serves as the initial guess of the concentration profiles of individual components. Following this, MCR-ALS procedure can be applied in which (1) is iteratively solved to determine spectral (S) and concentration (C) profiles of individual components. It should be emphasized that MCR-ALS is based on bilinear model according to which $\mathbf{D_i}$ matrix can be obtained as product of two matrices and in which both concentration and spectral profiles should be imposed to possess only positive values (belong to $\mathbf{R}+$) using non-negativity constraint. Both EFA and MCR-ALS algorithms used to solve equation (1) are implemented in the publicly available Matlab-code [52] and further details on its usage can be found in [40,53,54].

As temperature-dependence of optical properties of a dielectric can be assessed by analyzing the spectral signatures using MCR-ALS with EFA [55,56] (see also Supporting Information, section S4), this tool can be used in discrimination of low- and high-temperature component behavior as well. Displaying non-linear behavior as the temperature rises, the concentration profiles of low- and high-temperature component correspond to high- and low-density water, respectively [57–60]. The regression of these data sets on the 2nd degree polynomial ($y = B_0 + B_1 \cdot x + B_2 \cdot x^2$) provides three, in physical sense rather abstract parameters, but mathematically significant: B_0 indicates relative concentration of particular component at 0 °C, B_1 suggests the rate of a decrease of particular component at the expense of another one and B_2 stems from the curvature of the profile, serving as a metric via which one can monitor particular alterations occurring in the low-/high-density components with the change in temperature . Importantly, it is necessary to point out that, although the obtained parameters indeed correlate with the aforementioned physical quantities, the two are not in a bijective relationship, as can be easily observed from the behavior of high-density water B_0 coefficient, whose value is consistently negative. This behavior of the B_0 coefficient stems from both the fitting procedure and the multivariate analysis, which is performed without imposing any boundary conditions, in order to obtain as unbiased results as possible. Thus, even though the obtained coefficients cannot, in general, be interpreted in terms of physical

quantities, this does not diminish the validity of the subsequent analysis, being based not on the absolute values of the obtained coefficients, but rather on the comparison between them. Since the temperature-dependent fluctuations of a hydrogen bond network are presumably reflected in different behavior of low- and high-temperature components (high- and low-density water, respectively), they can be identified by the appearance of the asymmetry in these two components. Thus, only the values and eventual differences in parameters obtained from fitting these two curves should matter; parameter values obtained from concentration profiles of low- and high-temperature components very likely reflect the presence of a particular ion, whereas their difference suggests asymmetry, i.e. in the absence of the asymmetry there are either no temperature-dependent fluctuations in the system or the fluctuations are undetectable by analyzing this particular vibrational band / spectral region.

3. Results and discussion

3.1 Univariate analysis

Water combination band, with its maximum appearing at about 2130 cm^{-1}, displays absorbance decrease and low-frequency shift as the temperature rises. Baseline-corrected spectra of NaCl and NaI, and also KCl and KI (solid lines) in D_1 spectral range are presented in Fig. 1a and 1b, along with their S profiles (low- and high-temperature components that correspond to the spectra of high- and low-density water [15,16] (labelled with dotted curves) which is discussed section 3.2 (analogous spectra of the remaining salts are not displayed, since, in qualitative terms, they are virtually indistinguishable). As demonstrated previously [46], ν_{max} reflects the impact of a certain ion on a hydrogen bond network. In contrast to the study conducted by Verma et al. [46], we are comparing this parameter in equivalent systems, i.e. those recorded at the same ionic strength and in the same temperature range. By measuring ν_{max} at a certain temperature we are able to extrapolate the position of the band maximum at zero ($\nu_{max,\,0}$) at which librations are expected to be significantly lower [5], and the analyzed band should reflect only the instantaneous arrangement of water molecules and corresponding hydrogen bond network. As seen from Fig. 1c and 1d, the salts NaCl, NaI, KCl and KI in the absence of librations generate band with the maximum at different positions: $\nu_{max,\,0}$= 2140.3 ± 0.2 cm^{-1} for NaCl, 2140.6 ± 0.3 cm^{-1} for KCl, 2135.2 ± 0.2 cm^{-1} for NaI and 2133.7 ± 0.4 cm^{-1} for KI (see Table 1). This observation suggests that ν_{max}

differences between the salts are similar for Na^+ and K^+ and, consequently, are primarily driven by the difference in present anionic species. According to the analogous quantity determined form the solutions of the remaining salts (Table 1), this appears to be the general case. When the anions are ordered by the position of $\nu_{max,\,0}$ we obtain the following series: $CH_3COO^- > H_2O > NO_2^- > NO_3^- > Cl^- > Br^- > I^-$. The order of anions suggests that the hydrogen bond network formed between water molecules and anions (investigated cations, due to their effectively identical influence on the band, can be considered as the constant term, i.e. taken out of consideration) is governed by electrostatic interactions [47,48]. More precisely, monopole (halide ions) – dipole (H_2O) interaction represents one extreme, with the behavior slightly shifting in the case of hetermolecular dipole (NO_2^- / NO_3^-) – dipole (H_2O) and homomolecular dipole (H_2O) – dipole (H_2O) interactions all the way to the opposite extreme, namely acetate (CH_3COO^-) – H_2O. This latter extreme is gravely influenced by hydrophobic hydration, in which CH_3 moiety induces different and specific clustering of water molecules in its vicinity, with the effect subsequently propagating to the entire water hydrogen bond network [39,61,62].

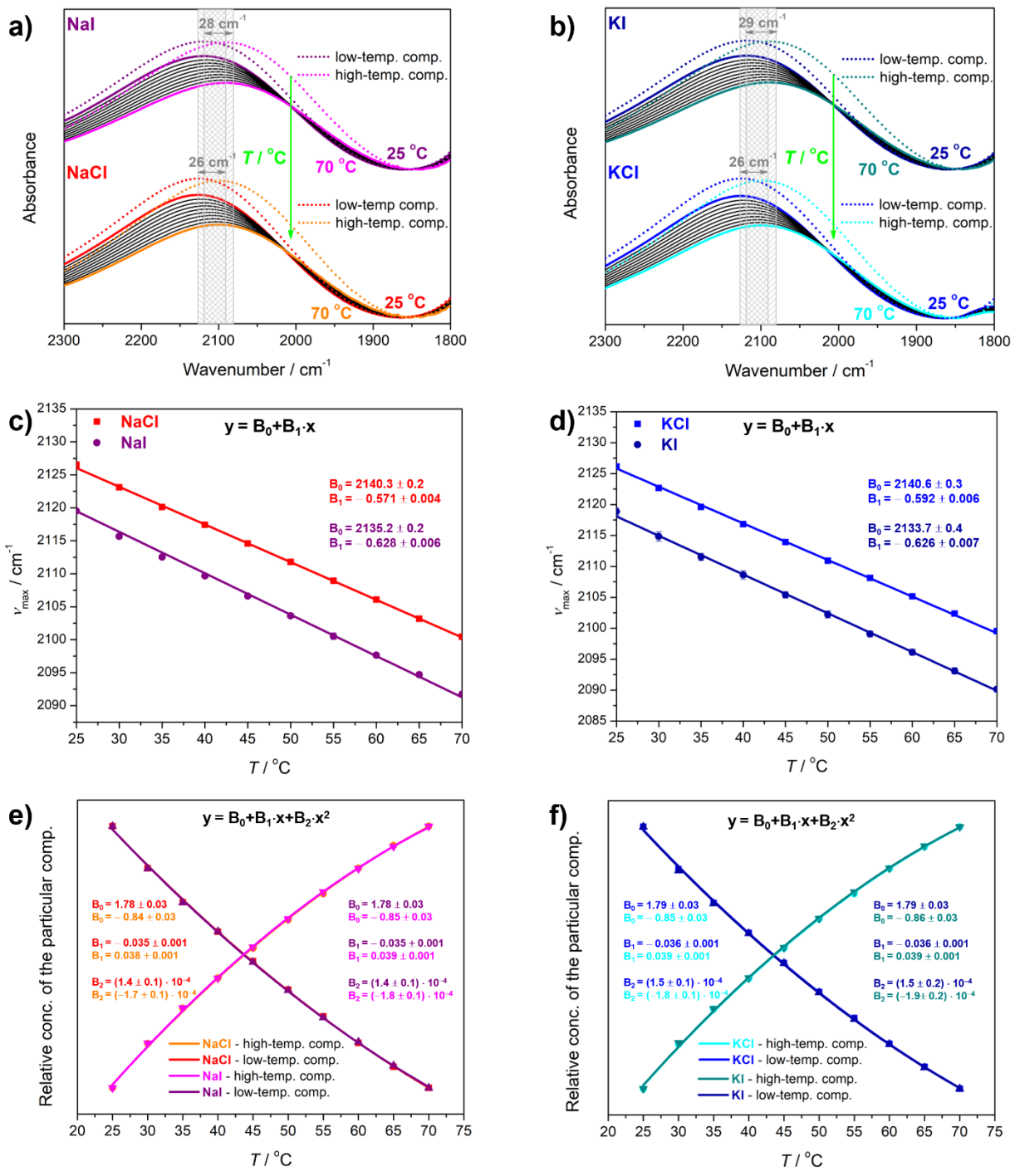

Fig. 1. Temperature-dependent FT-IR spectra (25-70 °C) in the spectral region 2300 to 1800 cm^{-1} of: a) NaI (25 °C purple line, 70 °C magenta line) and NaCl (25 °C red line, 70 °C orange line) and b) KI (25 °C royal line, 70 °C dark cyan line) and KCl (25 °C blue line, 70 °C cyan line). Spectral profiles of low- and high-temperature component are labelled by dotted lines with

corresponding colors, respectively; Univariate analysis of ν_{max} (cm^{-1}) results of c) NaI and NaCl and d) KI and KCl.; Multivariate analysis of IR spectra of: e) NaI (low-temp. comp. (purple) and high-temp. comp. (magenta)) and NaCl (low-temp. comp. (red) and high-temp. comp. (orange)) and f) KI (low-temp. comp. (royal) and high-temp. comp. (dark cyan)) and KCl (low-temp. comp. (blue) and high-temp. comp. (cyan)). Results stemming from fitting procedure (linear for c) and d) and parabolic for e) and f)) are displayed in graphs.

Regarding the slope of this line (B_1), it is less informative than B_0. The steepest slope is found for H_2O (-0.678 ± 0.004 cm^{-1} $°C^{-1}$), with the shallowest one appearing in the case of NaCl solution (-0.571 ± 0.004 cm^{-1} $°C^{-1}$). Although the uncertainties in the slopes are rather minute, they all can be treated as 0.6 cm^{-1} $°C^{-1}$. In the physical context the slope can be considered as the rate of the change of the hydrogen bond network with the temperature or, simply, as the temperature-dependent fluctuations of a hydrogen bond network. In order to unravel eventual ion-induced perturbations in temperature-dependent behavior of the hydrogen bond network, a completely different perspective on the data is necessary, invoking multivariate analysis approach.

3. 2 Multivariate analysis

The application of MCR-ALS with EFA on D_1 spectral range provided spectral signatures of the two resolved components, namely low-and high-temperature components corresponding to the high-density water and low-density water [15], respectively (these terms will be used interchangeably through the text). Their spectral profiles are presented as dotted lines on Fig. 1a (NaCl – red and orange, NaI – purple and magenta) and b) (KCl – blue and cyan, KI – royal and dark cyan). Values of the band maxima of spectral profiles ($\nu_{max,\,S1\,/\,S2}$) of all systems are displayed in Table S2 (section S5) in Supporting Information as well as the example of residuals (section S6). Their concentration profiles, presented in Fig. 1e and 1f, showcase the appearance of non-linearity, reflecting temperature-dependent nature of water density [57,63,64]. By examining the results of the performed fitting procedure, we obtain values representing intercept (B_0), slope (B_1 in $°C^{-1}$) and curvature (B_2 in $°C^{-2}$). In the remainder of the manuscript only the behavior of the absolute values of the parameters representing the slope and the curvature, namely $|B_1|$ and $|B_2|$, are considered.

As displayed in Table 1, B_0 (*y*-intercept) values of all concentration profiles are approximately 1.8 for high-density water and −0.8 for low-density water. Interestingly, the slopes (B_1 parameters) of these two curves display slight asymmetry: on average, it is approximately |0.004| in $°C^{-1}$, even with the combined experimental/analytical uncertainty taken into account. Furthermore, consistent and ion-independent asymmetry in $|B_2|$ values is observed as well ((0.3 - 0.4) $\cdot 10^{-4}$ $°C^{-2}$); additionally, certain trend emerges. $|B_2|$ values of low-density water of Na^+ and K^+ halides range from $(1.4 \pm 0.2) \cdot 10^{-4}$ $°C^{-2}$ to $(1.5 \pm 0.2) \cdot 10^{-4}$ $°C^{-2}$, and for high-density water from $(1.7 \pm 0.2) \cdot 10^{-4}$ $°C^{-2}$ to $(1.8 \pm 0.2) \cdot 10^{-4}$ $°C^{-2}$. Analogous quantities for nitrates ($NaNO_3$ and KNO_3) are $(1.6 \pm 0.2) \cdot 10^{-4}$ $°C^{-2}$ for low-density water and $(1.9 \pm 0.2) \cdot 10^{-4}$ $°C^{-2}$ to $(2.0 \pm 0.2) \cdot 10^{-4}$ $°C^{-2}$ for high-density water. For salts of strong bases (NaOH / KOH) and weak acids (HNO_2 and CH_3COOH) $|B_2|$ values are quite similar, $(1.9 \pm 0.2) \cdot 10^{-4}$ $°C^{-2}$ for low-density water and about $(2.0 \pm 0.2) \cdot 10^{-4}$ $°C^{-2}$ for high-density water.

Due to rather minor differences in the non-linear parameter $|B_2|$ between different salts, one cannot discriminate different solutions based on this metric. Bearing this in mind we focus solely on the asymmetry in $|B_2|$ obtained from the behavior of high- and low-density water in the case of each solution. Asymmetry usually refers to the difference in the system behavior when it responds on the temperature change in two opposite directions (heating – cooling). In the systems examined in this study the asymmetry between high- and low-density water can be interpreted in terms of different response of the hydrogen bond network to the heating and cooling, or, more specifically, asymmetry appears due to temperature-dependent fluctuations in water hydrogen bond network. Being free from any possible underlying assumption on the arrangement of water molecules in water hydrogen bond network, hereafter we discuss only the differences in $|B_2|$ coefficients for high- and low-density water and label this difference as asymmetry. As seen from H_2O, the asymmetry between high- and low-density water is ~ $|0.4| \cdot 10^{-4}$ $°C^{-2}$ (Table 1). In spite of relatively minor differences in $|B_2|$ coefficients when comparing solutions of different salts, asymmetry is seen in aqueous solutions of all investigated salts, with the found asymmetry being virtually identical (Table 1), suggesting that it is independent of the dissolved salt. This finding is rather important as it implies that the temperature-dependent fluctuations of water hydrogen bond network, at moderate pH values (see Supporting Information, sections S2 and S7), are ion-invariant even in the high ionic strength regime.

As the examined band (D_1 spectral range) originates from the combination of a fundamental transition (1←0) of δHOH and water libration ($\rho_L H_2O$), the former being intramolecular and the latter intermolecular vibrational mode, we ultimately confirm that librations are more sensitive to the associated fluctuations of hydrogen bond network, and can thus indeed serve as a descriptor of this phenomenon [5]. Since this spectral region differs from all the others in Mid-IR ≥ 1000 cm^{-1} by possessing the signature of water librations, we examined the spectral range in which the latter is absent in order to ensure that librations are indeed responsible for the observed asymmetry. In this respect, we examined the region (D_2) where only partial signature of linear bending is captured (Fig. 2a, 2b).

Table 1. Parameters obtained from linear (B_0, B_1) and non-linear (B_0, B_1, B_2) regression of the results produced by uni- and multivariate analysis conducted on D_1 and on D_1 and D_2 spectral ranges, respectively (salts are ordered by descending values of B_0 obtained from univariate analysis).

system	Univariate analysis		Multivariate analysis (MCR-ALS with EFA)					
			2300-1800 cm^{-1} (D_1)			1560-1260 cm^{-1} (D_2)		
	B_0[a]	B_1[b]	B_0[c]	B_1[d]	B_2[e] $\cdot 10^4$	B_0[c]	B_1[d]	B_2[e] $\cdot 10^4$
KI	2133.7 ± 0.4	–0.626 ± 0.007	1.79 ± 0.03 –0.86 ± 0.03	–0.036 ± 0.001 0.039 ± 0.001	1.5 ± 0.2 –1.8 ± 0.2	1.73 ± 0.03 –0.73 ± 0.03	–0.032 ± 0.001 0.032 ± 0.001	1.1 ± 0.1 –1.1 ± 0.1
NaI	2135.2 ± 0.2	–0.628 ± 0.006	1.78 ± 0.03 –0.85 ± 0.03	–0.035 ± 0.001 0.039 ± 0.001	1.4 ± 0.1 –1.8 ± 0.1	1.70 ± 0.03 –0.70 ± 0.03	–0.031 ± 0.001 0.031 ± 0.001	1.0 ± 0.1 –1.0 ± 0.1
KBr	2136.9 ± 0.3	–0.608 ± 0.006	1.79 ± 0.03 –0.84 ± 0.03	–0.036 ± 0.001 0.039 ± 0.001	1.5 ± 0.1 –1.8 ± 0.1	1.73 ± 0.02 –0.73 ± 0.02	–0.032 ± 0.001 0.032 ± 0.001	1.1 ± 0.1 –1.1 ± 0.1
NaBr	2139.4 ± 0.3	–0.600 ± 0.007	1.78 ± 0.03 –0.84 ± 0.04	–0.035 ± 0.001 0.039 ± 0.002	1.4 ± 0.2 –1.8 ± 0.2	1.69 ± 0.02 –0.69 ± 0.02	–0.030 ± 0.001 0.030 ± 0.001	1.0 ± 0.1 –1.0 ± 0.1
NaCl	2140.3 ± 0.2	–0.571 ± 0.004	1.78 ± 0.03 –0.84 ± 0.03	–0.035 ± 0.001 0.038 ± 0.001	1.4 ± 0.1 –1.7 ± 0.2	1.74 ± 0.03 –0.74 ± 0.03	–0.033 ± 0.001 0.033 ± 0.001	1.1 ± 0.2 –1.1 ± 0.1
KCl	2140.6 ± 0.3	–0.592 ± 0.006	1.79 ± 0.03 –0.85 ± 0.03	–0.036 ± 0.001 0.039 ± 0.001	1.5 ± 0.1 –1.8 ± 0.1	1.71 ± 0.02 –0.71 ± 0.02	–0.031 ± 0.001 0.031 ± 0.001	1.0 ± 0.1 –1.0 ± 0.1
KOH	2142.7 ± 0.4	–0.63 ± 0.01	1.82 ± 0.03 –0.86 ± 0.03	–0.037 ± 0.002 0.039 ± 0.001	1.6 ± 0.2 –1.9 ± 0.1			
$NaNO_3$	2142.8 ± 0.3	–0.604 ± 0.007	1.80 ± 0.04 –0.86 ± 0.04	–0.037 ± 0.001 0.040 ± 0.002	1.6 ± 0.2 –1.9 ± 0.2	n. a.		
KNO_3	2143 ± 0.3	–0.628 ± 0.006	1.82 ± 0.03 –0.88 ± 0.03	–0.037 ± 0.001 0.041 ± 0.001	1.6 ± 0.1 –2.0 ± 0.1			

system	Univariate analysis		Multivariate analysis (MCR-ALS with EFA)					
			2300-1800 cm^{-1} (D_1)			1560-1260 cm^{-1} (D_2)		
	B_0[a]	B_1[b]	B_0[c]	B_1[d]	B_2[e] $\cdot 10^4$	B_0[c]	B_1[d]	B_2[e] $\cdot 10^4$
NaOH	2143.6 ± 0.2	–0.657 ± 0.006	1.83 ± 0.01	–0.037 ± 0.001	1.6 ± 0.1			
			–0.90 ± 0.02	0.041 ± 0.001	–2.0 ± 0.1			
KNO_2	2147.6 ± 0.3	–0.641 ± 0.007	1.83 ± 0.03	–0.038 ± 0.001	1.7 ± 0.1			
			–0.87 ± 0.03	0.040 ± 0.002	–2.0 ± 0.2		n. a.	
$NaNO_2$	2148.6 ± 0.3	–0.646 ± 0.008	1.84 ± 0.04	–0.038 ± 0.002	1.7 ± 0.2			
			–0.89 ± 0.04	0.041 ± 0.002	–2.0 ± 0.2			
H_2O	2152.5 ± 0.2	–0.678 ± 0.004	1.80 ± 0.03	–0.036 ± 0.001	1.5 ± 0.1	1.69 ± 0.02	–0.030 ± 0.001	0.82 ± 0.01
			–0.87 ± 0.03	0.040 ± 0.001	–1.9 ± 0.1	–0.69 ± 0.02	0.030 ± 0.001	–0.83 ± 0.01
CH_3COONa	2156 ± 0.2	–0.626 ± 0.004	1.82 ± 0.04	–0.038 ± 0.002	1.7 ± 0.2			
			–0.89 ± 0.04	0.042 ± 0.002	–2.1 ± 0.2		n. a.	
CH_3COOK	2156.4 ± 0.2	–0.596 ± 0.003	1.82 ± 0.02	–0.037 ± 0.001	1.6 ± 0.1			
			–0.88 ± 0.02	0.041 ± 0.001	–2.0 ± 0.1			

[a] In cm^{-1}; [b] In cm^{-1} °C^{-1}; [c] Dimensionless quantity; [d] In °C^{-1}; [e] °C^{-2}; n. a. stands for not analyzed (see Supporting Information, sections S7 and S8, for more details)

In this regard, we find that δHOH band (D_2) displays small low-wavenumber shift as temperature rises with its intensity only slightly rising [46], whereas the low-wavenumber shift of a combination band is accompanied with greater absorbance decrease.

In Fig. 2a and 2b are displayed FT-IR spectra of water solutions that contain partial signature of δHOH in temperature range 25-70 °C. We excluded aqueous solutions of salts which are constituted from ions displaying signatures in this spectral region (see Supporting Information, sections S7 and S8 for more details); thus, only salts of halide ions are displayed. By following the same MCR-ALS with EFA procedure as for D_1 spectral range, we obtained the parameters describing this region (presented in Table 1). We thereby find that $|B_0|$ coefficients are mutually very similar (1.69 - 1.74 and 0.69 - 0.74), while both $|B_1|$ (0.030 - 0.032 $°C^{-1}$) and $|B_2|$ ((1.0 - 1.1) $\cdot 10^{-4}$ $°C^{-2}$) are virtually identical for all aforementioned salts, respectively. We can thus conclude that, when the signal stemming from librations is absent, no asymmetry is observed from the concentration profiles of high- and low-density water.

It is worth mentioning that B_0 coefficients, which were not thoroughly discussed up to this point, exhibit particular symmetry in the case of D_2 region (see Table 1, see Fig. 2c and 2d). More precisely, in the case of all investigated salt solutions (and pure water) B_0 coefficients are perfectly symmetric around y = 0.5 (point denoting the mixture of low- and high-temperature water components in 1:1 ratio). This finding suggests two different conclusions; firstly, if the choice of two components indeed exhausts the component phase space, i.e. if two components are enough to completely describe the system at hand, one should expect that they possess virtually identical, albeit symmetrical appearance (mirror symmetry in B_0 coefficients and profiles around line y = 0.5 to be precise). Secondly, due to the fact that D_1 region does not exhibit this perfectly symmetrical behavior (while the difference in the average B_0 coefficients between two regions is rather minute, it is still significant), showing consistently distinct behavior compared to D_2 case. Thus, we find that even B_0 coefficients showcase the found asymmetry (albeit to a less significant extent) and reflect the difference in the temperature-dependent behavior of the two investigated spectral regions.

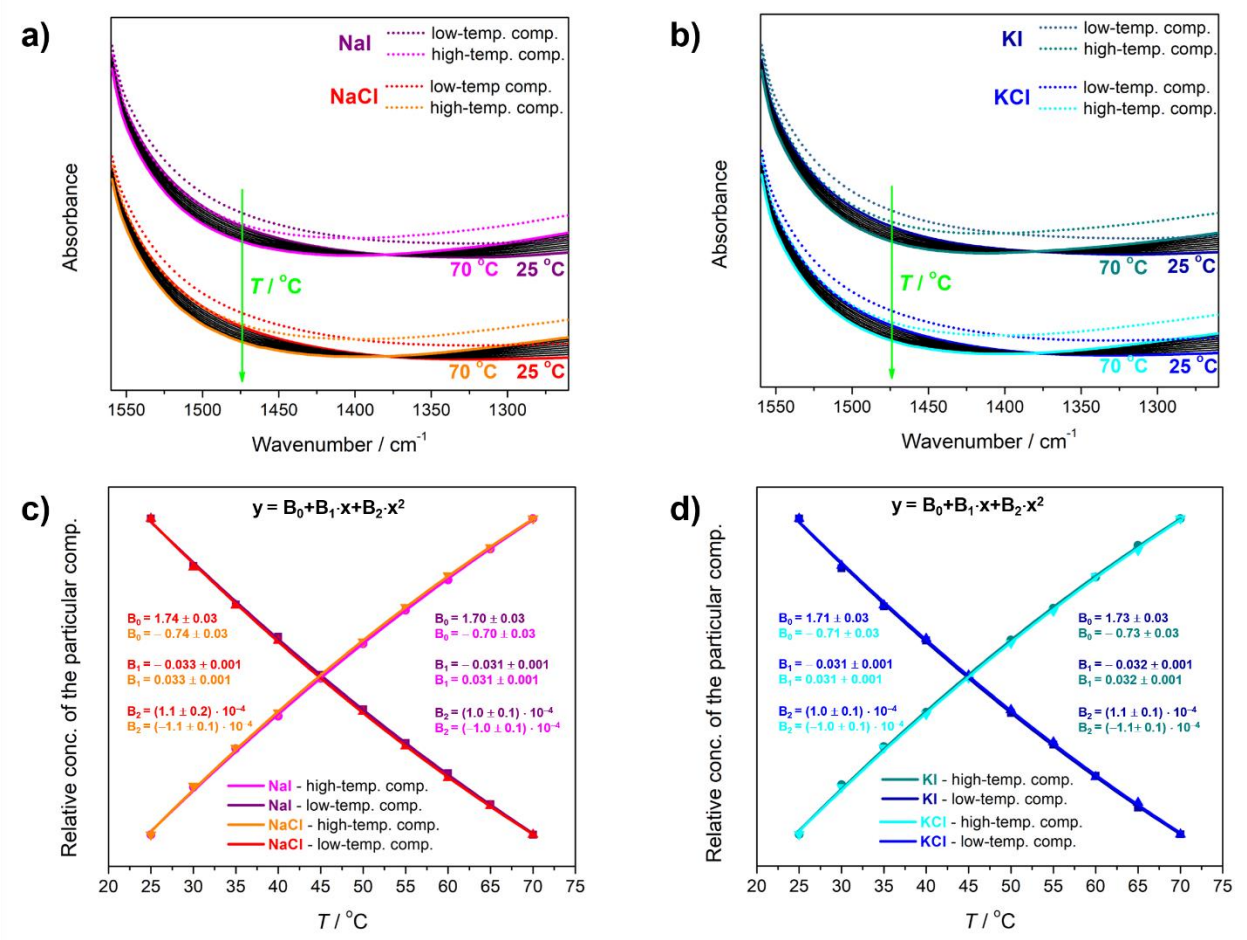

Fig. 2. Temperature-dependent FT-IR spectra (25-70 °C) in the spectral region 1560 to 1826 cm^{-1} of: a) NaI (25 °C purple line, 70 °C magenta line) and NaCl (25 °C red line, 70 °C orange line) and b) KI (25 °C royal line, 70 °C dark cyan line) and KCl (25 °C blue line, 70 °C cyan line). Spectral profiles of low- and high-temperature component are labelled by dotted lines with corresponding colors, respectively; Multivariate analysis of IR spectra of: c) NaI (low-temp. comp. (purple) and high-temp. comp. (magenta)) and NaCl (low-temp. comp. (red) and high-temp. comp. (orange)) and d) KI (low-temp. comp. (royal) and high-temp. comp. (dark cyan)) and KCl (low-temp. comp. (blue) and high-temp. comp. (cyan)). Fitting results are displayed in graphs.

Due to the fact that the only, and thereby key, difference between these two spectral regions is in the presence/absence of librations, direct implication is that the fluctuations of hydrogen bond network are indeed reflected through water librations. In the context of findings provided by

Libanu et al. [15] and Czarnik-Matusewicz et al. [16], one can tentatively conclude that low- and high-density water possesses different rearrangement times on average; importantly, this reorganization seems to be independent on the presence of ions. Of course, this phenomenon could express different behavior for larger and structurally more diverse solutes that can be involved in additional directed interactions to much greater extent, in which cooperative effects might play significant role (lipids, for instance). Since the fluctuations in a hydrogen bond network are recognized as crucial events for electron transfer in various biochemical processes [65], the study presented in this manuscript serves as a seed for examining aqueous solution of more complex biologically relevant systems, e.g. sugars. Ultimately, this study shows that certain phenomena, accessible up to now only by time-resolved spectroscopic techniques, can be characterized and discerned with a combination of significantly simpler spectroscopic technique and an appropriate chemometric tool [49,66].

Conclusion

Temperature-dependent FT-IR spectra of aqueous solutions of monovalent salts were examined in two spectral ranges; the one in which water combination band appears and the region containing partial signature of water linear bending. Univariate analysis of the combination band revealed that the interaction of water and anions are primarily governed by their electrostatic interactions. Using MCR-ALS with EFA non-linear concentration profiles of high- and low-density water were obtained in both spectral ranges. The asymmetry in their behavior in the first spectral range, which is absent in the second spectral range, is assigned to the fluctuations in water hydrogen bond network. As the asymmetry is virtually indistinguishable for all investigated salts, we conclude that the fluctuations in water hydrogen bond network are ion-invariant, even in the regime of high ionic strengths. In technically significantly less demanding and more straightforward way, which is complemented by appropriate chemometric technique, our results confirm previous reports obtained by time-resolved spectroscopy and provide new means in deciphering this phenomenon.

Acknowledgment

This article was supported by the Croatian Science Foundation, Project No. UIP-2020-02-7669. The authors wish to express their gratitude to the Laboratory for Biomimetic Chemistry and Laboratory for Biomolecular Interactions and Spectroscopy (Ruđer Bošković Institute) for

providing the chemicals, as well as to the Laboratory for Physical Organic Chemistry (Ruđer Bošković Institute) for utilizing FT-IR spectrometer with ATR unit for acquiring the FT-IR spectra of powders (the data are in Supporting Information).

Supporting Information

Supporting Information associated with this paper can be found in the online version at http://.

References:

[1] J.A. Faust, J.P.S. Wong, A.K.Y. Lee, J.P.D. Abbatt, Role of Aerosol Liquid Water in Secondary Organic Aerosol Formation from Volatile Organic Compounds, Environ. Sci. Technol. 51 (2017) 1405–1413. https://doi.org/10.1021/acs.est.6b04700.

[2] S.M.M. Uddin, R.J. Harper, D.J. Henry, Contribution of Binary Organic Layers to Soil Water Repellency: A Molecular Level Perspective, J. Phys. Chem. A. 123 (2019) 7518–7527. https://doi.org/10.1021/acs.jpca.9b04033.

[3] P. Jungwirth, Biological Water or Rather Water in Biology?, J. Phys. Chem. Lett. 6 (2015) 2449–2451. https://doi.org/10.1021/acs.jpclett.5b01143.

[4] E. Brini, C.J. Fennell, M. Fernandez-Serra, B. Hribar-Lee, M. Lukšič, K.A. Dill, How Water's Properties Are Encoded in Its Molecular Structure and Energies, Chem. Rev. 117 (2017) 12385–12414. https://doi.org/10.1021/acs.chemrev.7b00259.

[5] Y. Maréchal, The Hydrogen Bond and the Water Molecule, Elsevier, 2007. https://www.sciencedirect.com/book/9780444519573/the-hydrogen-bond-and-the-water-molecule#book-info.

[6] A. Nilsson, L.G.M. Pettersson, The structural origin of anomalous properties of liquid water, Nat. Commun. 6 (2015). https://doi.org/10.1038/ncomms9998.

[7] F. Cipcigan, V. Sokhan, G. Martyna, J. Crain, Structure and hydrogen bonding at the limits of liquid water stability, Sci. Rep. 8 (2018) 1–8. https://doi.org/10.1038/s41598-017-18975-7.

[8] Y. Gao, H. Fang, K. Ni, A hierarchical clustering method of hydrogen bond networks in

liquid water undergoing shear flow, Sci. Rep. 11 (2021) 1–14. https://doi.org/10.1038/s41598-021-88810-7.

[9] A. Nilsson, C. Huang, L.G.M. Pettersson, Fluctuations in ambient water, J. Mol. Liq. 176 (2012) 2–16. https://doi.org/10.1016/j.molliq.2012.06.021.

[10] G. Camisasca, D. Schlesinger, I. Zhovtobriukh, G. Pitsevich, L.G.M. Pettersson, A proposal for the structure of high- and low-density fluctuations in liquid water, J. Chem. Phys. 151 (2019). https://doi.org/10.1063/1.5100875.

[11] Y. Maréchal, The molecular structure of liquid water delivered by absorption spectroscopy in the whole IR region completed with thermodynamics data, J. Mol. Struct. 1004 (2011) 146–155. https://doi.org/10.1016/j.molstruc.2011.07.054.

[12] J.D. Eaves, J.J. Loparo, C.J. Fecko, S.T. Roberts, A. Tokmakoff, P.L. Geissler, Hydrogen bonds in liquid water are broken only fleetingly, Proc. Natl. Acad. Sci. U. S. A. 102 (2005) 13019–13022. https://doi.org/10.1073/pnas.0505125102.

[13] P. Larouche, J.J. Max, C. Chapados, Isotope effects in liquid water by infrared spectroscopy. II. Factor analysis of the temperature effect on H2 O and D2 O, J. Chem. Phys. 129 (2008). https://doi.org/10.1063/1.2960583.

[14] F.O. Libnau, O.M. Kvalheim, A.A. Christy, J. Toft, Spectra of water in the near- and mid-infrared region, Vib. Spectrosc. 7 (1994) 243–254. https://doi.org/10.1016/0924-2031(94)85014-3.

[15] F.O. Libnau, J. Toft, A.A. Christy, O.M. Kvalheim, Structure of Liquid Water Determined from Infrared Temperature Profiling and Evolutionary Curve Resolution, J. Am. Chem. Soc. 116 (1994) 8311–8316. https://doi.org/10.1021/ja00097a043.

[16] B. Czarnik-Matusewicz, S. Pilorz, J.P. Hawranek, Temperature-dependent water structural transitions examined by near-IR and mid-IR spectra analyzed by multivariate curve resolution and two-dimensional correlation spectroscopy, Anal. Chim. Acta. 544 (2005) 15–25. https://doi.org/10.1016/j.aca.2005.04.040.

[17] J.D. Smith, C.D. Cappa, K.R. Wilson, R.C. Cohen, P.L. Geissler, R.J. Saykally, Unified

description of temperature-dependent hydrogen-bond rearrangements in liquid water, Proc. Natl. Acad. Sci. U. S. A. 102 (2005) 14171–14174. https://doi.org/10.1073/pnas.0506899102.

[18] J.D. Smith, C.D. Cappa, K.R. Wilson, B.M. Messer, R.C. Cohen, R.J. Saykally, Energetics of hydrogen bond network rearrangements in liquid water, Science (80-.). 306 (2004) 851–853. https://doi.org/10.1126/science.1102560.

[19] P. Wernet, D. Nordlund, U. Bergmann, M. Cavalleri, N. Odelius, H. Ogasawara, L.Å. Näslund, T.K. Hirsch, L. Ojamäe, P. Glatzel, L.G.M. Pettersson, A. Nilsson, The Structure of the First Coordination Shell in Liquid Water, Science (80-.). 304 (2004) 995–999. https://doi.org/10.1126/science.1096205.

[20] T. Morawietz, O. Marsalek, S.R. Pattenaude, L.M. Streacker, D. Ben-Amotz, T.E. Markland, The Interplay of Structure and Dynamics in the Raman Spectrum of Liquid Water over the Full Frequency and Temperature Range, J. Phys. Chem. Lett. 9 (2018) 851–857. https://doi.org/10.1021/acs.jpclett.8b00133.

[21] S. Shimizu, N. Matubayasi, Ion hydration: Linking self-diffusion and reorientational motion to water structure, Phys. Chem. Chem. Phys. 20 (2018) 5909–5917. https://doi.org/10.1039/c7cp07309g.

[22] E. Lee, J.H. Choi, M. Cho, The effect of Hofmeister anions on water structure at protein surfaces, Phys. Chem. Chem. Phys. 19 (2017) 20008–20015. https://doi.org/10.1039/c7cp02826a.

[23] D. Laage, J.T. Hynes, Reorientional dynamics of water molecules in anionic hydration shells, Proc. Natl. Acad. Sci. U. S. A. 104 (2007) 11167–11172. https://doi.org/10.1073/pnas.0701699104.

[24] L. Comez, M. Paolantoni, P. Sassi, S. Corezzi, A. Morresi, D. Fioretto, Molecular properties of aqueous solutions: A focus on the collective dynamics of hydration water, Soft Matter. 12 (2016) 5501–5514. https://doi.org/10.1039/c5sm03119b.

[25] G. Stirnemann, E. Wernersson, P. Jungwirth, D. Laage, Mechanisms of acceleration and

retardation of water dynamics by ions, J. Am. Chem. Soc. 135 (2013) 11824–11831. https://doi.org/10.1021/ja405201s.

[26] J.J. Max, C. Chapados, IR spectroscopy of aqueous alkali halide solutions: Pure salt-solvated water spectra and hydration numbers, J. Chem. Phys. 115 (2001) 2664–2675. https://doi.org/10.1063/1.1337047.

[27] J.J. Max, V. Gessinger, C. Van Driessche, P. Larouche, C. Chapados, Infrared spectroscopy of aqueous ionic salt solutions at low concentrations, J. Chem. Phys. 126 (2007). https://doi.org/10.1063/1.2717184.

[28] J.J. Max, C. Chapados, Infrared spectroscopy of aqueous ionic salt mixtures at low concentrations: Ion pairing in water, J. Chem. Phys. 127 (2007). https://doi.org/10.1063/1.2764485.

[29] F. Rauh, B. Mizaikoff, Simultaneous Determination of Monoatomic Ions via Infrared Attenuated Total Reflection Spectroscopy in Aqueous Solution at Different Temperatures, Appl. Spectrosc. 70 (2016) 1214–1227. https://doi.org/10.1177/0003702816652320.

[30] B. Kang, H. Tang, Z. Zhao, S. Song, Hofmeister Series: Insights of Ion Specificity from Amphiphilic Assembly and Interface Property, ACS Omega. 5 (2020) 6229–6239. https://doi.org/10.1021/acsomega.0c00237.

[31] M.A. Metrick, N. do Carmo Ferreira, E. Saijo, A.G. Hughson, A. Kraus, C. Orrú, M.W. Miller, G. Zanusso, B. Ghetti, M. Vendruscolo, B. Caughey, Million-fold sensitivity enhancement in proteopathic seed amplification assays for biospecimens by Hofmeister ion comparisons, Proc. Natl. Acad. Sci. U. S. A. 116 (2019) 23029–23039. https://doi.org/10.1073/pnas.1909322116.

[32] A. Mudi, C. Chakravarty, Effect of ionic solutes on the hydrogen bond network dynamics of water: Power spectral analysis of aqueous NaCl solutions, J. Phys. Chem. B. 110 (2006) 8422–8431. https://doi.org/10.1021/jp056003l.

[33] L.M. Pegram, M.T. Record, Quantifying accumulation or exclusion of H^+, HO^-, and Hofmeister salt ions near interfaces, Chem. Phys. Lett. 467 (2008) 1–8.

https://doi.org/10.1016/j.cplett.2008.10.090.

[34] H.I. Okur, J. Hladílková, K.B. Rembert, Y. Cho, J. Heyda, J. Dzubiella, P.S. Cremer, P. Jungwirth, Beyond the Hofmeister Series: Ion-Specific Effects on Proteins and Their Biological Functions, J. Phys. Chem. B. 121 (2017) 1997–2014. https://doi.org/10.1021/acs.jpcb.6b10797.

[35] S.T.V. Der Post, H.J. Bakker, The combined effect of cations and anions on the dynamics of water, Phys. Chem. Chem. Phys. 14 (2012) 6280–6288. https://doi.org/10.1039/c2cp23882a.

[36] S. Han, Anionic effects on the structure and dynamics of water in superconcentrated aqueous electrolytes, RSC Adv. 9 (2019) 609–619. https://doi.org/10.1039/c8ra09589b.

[37] J. Riemenschneider, J. Holzmann, R. Ludwig, Salt effects on the structure of water probed by attenuated total reflection infrared spectroscopy and molecular dynamics simulations, ChemPhysChem. 9 (2008) 2731–2736. https://doi.org/10.1002/cphc.200800571.

[38] Q. Zhang, Z. Pan, L. Zhang, R. Zhang, Z. Chen, T. Jin, T. Wu, X. Chen, W. Zhuang, Ion effect on the dynamics of water hydrogen bonding network: A theoretical and computational spectroscopy point of view, Wiley Interdiscip. Rev. Comput. Mol. Sci. 8 (2018) 1–23. https://doi.org/10.1002/wcms.1373.

[39] D. Ben-Amotz, Hydration-Shell Vibrational Spectroscopy, J. Am. Chem. Soc. 141 (2019) 10569–10580. https://doi.org/10.1021/jacs.9b02742.

[40] K.R. Fega, D.S. Wilcox, D. Ben-Amotz, Application of Raman multivariate curve resolution to solvation-shell spectroscopy, Appl. Spectrosc. 66 (2012) 282–288. https://doi.org/10.1366/11-06442.

[41] T. Seki, K.Y. Chiang, C.C. Yu, X. Yu, M. Okuno, J. Hunger, Y. Nagata, M. Bonn, The bending mode of water: A powerful probe for hydrogen bond structure of aqueous systems, J. Phys. Chem. Lett. 11 (2020) 8459–8469. https://doi.org/10.1021/acs.jpclett.0c01259.

[42] S.Y. Venyaminov, F.G. Prendergast, Water (H_2O and D_2O) molar absorptivity in the 1000-4000 cm^{-1} range and quantitative infrared spectroscopy of aqueous solutions, Anal.

Biochem. 248 (1997) 234–245. https://doi.org/10.1006/abio.1997.2136.

[43] C.C. Yu, K.Y. Chiang, M. Okuno, T. Seki, T. Ohto, X. Yu, V. Korepanov, H. o. Hamaguchi, M. Bonn, J. Hunger, Y. Nagata, Vibrational couplings and energy transfer pathways of water's bending mode, Nat. Commun. 11 (2020) 1–8. https://doi.org/10.1038/s41467-020-19759-w.

[44] Y. Tong, T. Kampfrath, R.K. Campen, Experimentally probing the libration of interfacial water: The rotational potential of water is stiffer at the air/water interface than in bulk liquid, Phys. Chem. Chem. Phys. 18 (2016) 18424–18430. https://doi.org/10.1039/c6cp01004k.

[45] M. Huš, T. Urbic, Strength of hydrogen bonds of water depends on local environment, J. Chem. Phys. 136 (2012) 1–7. https://doi.org/10.1063/1.3701616.

[46] P.K. Verma, A. Kundu, M.S. Puretz, C. Dhoonmoon, O.S. Chegwidden, C.H. Londergan, M. Cho, The Bend+Libration Combination Band Is an Intrinsic, Collective, and Strongly Solute-Dependent Reporter on the Hydrogen Bonding Network of Liquid Water, J. Phys. Chem. B. 122 (2018) 2587–2599. https://doi.org/10.1021/acs.jpcb.7b09641.

[47] H. Chen, M. Liu, T. Yan, Molecular multipoles and (hyper)polarizabilities from the Buckingham expansion: Revisited, Commun. Theor. Phys. 72 (2020). https://doi.org/10.1088/1572-9494/ab8a0d.

[48] A.D. Buckingham, H.C. Longuet-Higgins, The quadrupole moments of dipolar molecules, Mol. Phys. 14 (1968) 63–72. https://doi.org/10.1080/00268976800100051.

[49] Y. Chen, H.I. Okur, N. Gomopoulos, C. Macias-Romero, P.S. Cremer, P.B. Petersen, G. Tocci, D.M. Wilkins, C. Liang, M. Ceriotti, S. Roke, Electrolytes induce long-range orientational order and free energy changes in the H-bond network of bulk water, Sci. Adv. 2 (2016) 1–9. https://doi.org/10.1126/sciadv.1501891.

[50] F. Menges, Spectragryph - optical spectroscopy software, Version 1.2.15, 2015, http://www.effemm2.de/spectragryph/ (20.06.2021).

[51] H.R. Keller, D.L. Massart, Evolving factor analysis, Chemom. Intell. Lab. Syst. 12 (1991) 209–224. https://doi.org/10.1016/0169-7439(92)80002-L.

[52] J. Jaumot, R. Gargallo, A. De Juan, R. Tauler, A graphical user-friendly interface for MCR-ALS: A new tool for multivariate curve resolution in MATLAB, Chemom. Intell. Lab. Syst. 76 (2005) 101–110. https://doi.org/10.1016/j.chemolab.2004.12.007.

[53] A. De Juan, J. Jaumot, R. Tauler, Multivariate Curve Resolution (MCR). Solving the mixture analysis problem, Anal. Methods. 6 (2014) 4964–4976. https://doi.org/10.1039/c4ay00571f.

[54] M. Maeder, A. de Juan, Two-Way Data Analysis: Evolving Factor Analysis, Compr. Chemom. 2 (2009) 261–274. https://doi.org/10.1016/B978-044452701-1.00047-8.

[55] T. Sato, K. Katayama, Direct measurement of the propagation of the phase-transition region of liquid crystals, Sci. Rep. 7 (2017) 1–8. https://doi.org/10.1038/srep44801.

[56] P. Maleš, Z. Brkljača, I. Crnolatac, D. Bakarić, Application of MCR-ALS with EFA on FT-IR spectra of lipid bilayers in the assessment of phase transition temperatures: Potential for discernment of coupled events, Colloids Surfaces B Biointerfaces. 201 (2021). https://doi.org/10.1016/j.colsurfb.2021.111645.

[57] T.G. Mayerhöfer, A. Dabrowska, A. Schwaighofer, B. Lendl, J. Popp, Beyond Beer's Law: Why the Index of Refraction Depends (Almost) Linearly on Concentration, ChemPhysChem. 21 (2020) 707–711. https://doi.org/10.1002/cphc.202000018.

[58] T.G. Mayerhöfer, J. Popp, Beyond Beer's Law: Revisiting the Lorentz-Lorenz Equation, ChemPhysChem. 21 (2020) 1218–1223. https://doi.org/10.1002/cphc.202000301.

[59] A. Hitachi, V. Chepel, M.I. Lopes, V.N. Solovov, New approach to the calculation of the refractive index of liquid and solid xenon, J. Chem. Phys. 123 (2005) 1–7. https://doi.org/10.1063/1.2136879.

[60] T.G. Mayerhöfer, J. Popp, Beer's Law – Why Absorbance Depends (Almost) Linearly on Concentration, ChemPhysChem. 20 (2019) 511–515. https://doi.org/10.1002/cphc.201801073.

[61] D. Ben-Amotz, Hydrophobic ambivalence: Teetering on the edge of randomness, J. Phys. Chem. Lett. 6 (2015) 1696–1701. https://doi.org/10.1021/acs.jpclett.5b00404.

[62] J.G. Davis, K.P. Gierszal, P. Wang, D. Ben-Amotz, Water structural transformation at molecular hydrophobic interfaces, Nature. 491 (2012) 582–585. https://doi.org/10.1038/nature11570.

[63] E. Reisler, H. Eisenberg, A.P. Minton, Temperature and density dependence of the refractive index of pure liquids, J. Chem. Soc. Faraday Trans. 2 Mol. Chem. Phys. 68 (1972) 1001–1015. https://doi.org/10.1039/F29726801001.

[64] T.G. Mayerhöfer, J. Popp, Beer's law derived from electromagnetic theory, Spectrochim. Acta - Part A Mol. Biomol. Spectrosc. 215 (2019) 345–347. https://doi.org/10.1016/j.saa.2019.02.103.

[65] J.S. Kretchmer, N. Boekelheide, J.J. Warren, J.R. Winkler, H.B. Gray, T.F. Miller, Fluctuating hydrogen-bond networks govern anomalous electron transfer kinetics in a blue copper protein, Proc. Natl. Acad. Sci. U. S. A. 115 (2018) 6129–6134. https://doi.org/10.1073/pnas.1805719115.

[66] Y. Chen, N. Dupertuis, H.I. Okur, S. Roke, Temperature dependence of water-water and ion-water correlations in bulk water and electrolyte solutions probed by femtosecond elastic second harmonic scattering, J. Chem. Phys. 148 (2018). https://doi.org/10.1063/1.5023343.